organoids

MDPI

Article

Mimicking Senescence Factors to Characterize the Mechanisms Responsible for Hair Regression and Hair Loss: An In Vitro Study

Giacomo Masi, Camilla Guiducci and Francesca Rescigno *

VitroScreen Srl, Via Mosè Bianchi 103, 20149 Milan, Italy; giacomo.masi@vitroscreen.com (G.M.); camilla.guiducci@vitroscreen.com (C.G.)

* Correspondence: francesca.rescigno@vitroscreen.com

Abstract

Background/Objectives: VitroScreenORA® (by VitroScreen srl) Dermo Papilla spheroids, based on two micro-physiological systems (non-vascularized DP and vascularized VASC-DP), were used to study the molecular mechanisms behind hair cycle regression. Methods: Dermal papilla cells (HFDPC) were cultured to develop both models. Hair cycle regression was induced by exposing DP spheroids to TGF-β1 for 72 h and/or FGF-18 for an additional 24 h. Catagen phase entrance was evaluated by modulating specific genes (*FGF7*, *CCND1*, and *WNT5B*). The VASC-DP model was obtained by sequentially co-culturing HFDPC and primary dermal microvascular endothelial cells (HMDEC), mimicking the surrounding capillary loop. The vascular system's impact was assessed at 5 and 10 days using IF on CD31 (micro-vessels) and Fibronectin (FN). Nanostring nCounter® technology was applied to investigate the transcriptional signature based on the WNT pathway. Extended culture time up to 11 days simulated natural hair cycle regression, monitored by versican and FN expression (IF). Minoxidil, Doxorubicin, and Retinol-based products were used to modify physiological aging over time. Results: Data shows that the vascular system improves tissue physiology by modulating the associated genes. Extended culture time confirms progressive DP structure degeneration that is partially recoverable with Retinol-based treatments. Conclusions: Both models provide a reliable platform to investigate the hair cycle, paving the way for new testing systems for personalized therapies.

Keywords: hair follicle dermal papilla; 3D spheroid culture; endothelialization; wnt-signaling pathway; hair cycle

check for updates

Academic Editor: Süleyman Ergün

Received: 24 March 2025
Revised: 27 May 2025
Accepted: 1 July 2025
Published: 11 July 2025

Citation: Masi, G.; Guiducci, C.; Rescigno, F. Mimicking Senescence Factors to Characterize the Mechanisms Responsible for Hair Regression and Hair Loss: An In Vitro Study. *Organoids* **2025**, *4*, 17. https://doi.org/10.3390/organoids4030017

Copyright: © 2025 by the authors. Licensee MDPI, Basel, Switzerland. This article is an open access article distributed under the terms and conditions of the Creative Commons Attribution (CC BY) license (https://creativecommons.org/licenses/by/4.0/).

1. Introduction

The dermo-papillary unit is a complex anatomical structure located at the base of the hair follicle that plays a pivotal role in hair growth, regeneration, and overall skin health. Grasping the complexities of the dermal papilla's structure, function, and metabolism is crucial for uncovering the mechanisms behind hair disorders and for crafting innovative therapeutic strategies.

The hair follicle is a complex skin appendage composed of several cell types, but particularly by two main primary cellular elements: the hair follicle dermal papilla cells (HFDPCs) and the surrounding epidermal cells (ECs). The dynamic interaction between these connective and epithelial tissues is crucial for both the development and cyclical growth of hair [1–4]. The dermal papilla and dermal sheath originate from the dermal condensate, a group of mesenchymal cells that separates from the surrounding dermis during the initial stages of hair follicle development [5,6]. As the epidermis begins to

invaginate, dermal cells at the base of the developing follicle are enveloped by the epidermal cells, transforming into specialized fibroblasts of the dermal papilla. The interaction between the dermal papilla and the adjacent epithelium plays a pivotal role in inducing hair growth. The papilla's structure stimulates the epithelium to proliferate and differentiate, resulting in the formation of a hair fiber. Factors such as the size, shape, and interactions of the dermal papilla with the epidermis and the surrounding environment contribute to its functionality [7].

In mature hair follicles, the dermal papilla maintains and actively supports hair growth, while the interplay between mesenchymal and epithelial components drives hair cycle progression [8]. This cycle consists of three phases: anagen (growth), catagen (regression), and telogen (quiescence) [1,9,10] (Figure 1). A variety of growth factors and key cytokines, such as Wingless/Integrated (Wnt), Sonic Hedgehog (Shh), Ectodysplasin A (EDA), Bone Morphogenetic Protein (BMP), Transforming Growth Factor (TGF), and Fibroblast Growth Factor (FGF) signaling pathways, are involved in regulating these phases transitions controlling hair follicle maturation, proliferation, and differentiation with an impact on growth, color, shape, and size [7,11–17].

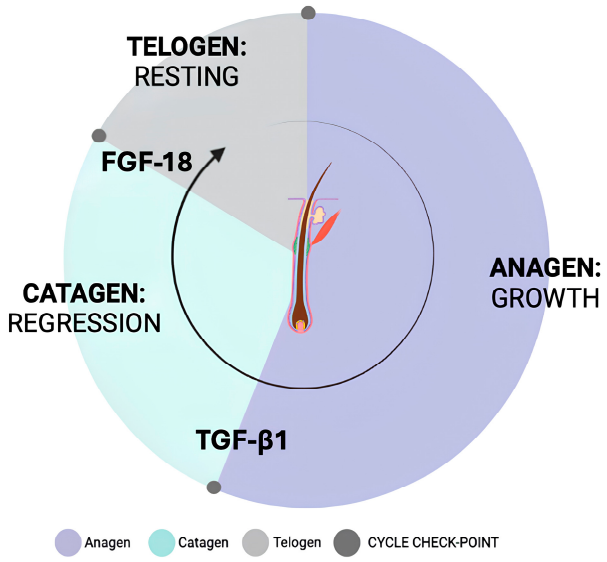


Figure 1. Schematic representation of the hair cycle.

The metabolic profile of the DP is highly dynamic and varies depending on the hair cycle stage. During the active growth phase of the hair cycle, known as the anagen phase, HFDPCs exhibit a high metabolic rate, characterized by increased glucose uptake and oxidative phosphorylation [18]. This metabolic shift provides the energy necessary for cell proliferation and differentiation. In contrast, in the regression and resting phases, named as the catagen and telogen phases, respectively, cells undergo a metabolic quiescence that exhibits a growth arrest [8,19]. During the anagen phase of the hair cycle, when hair growth is most active, angiogenesis, the formation of new blood vessels, is stimulated to support the increased metabolic activity of the follicle. This process is essential for maintaining sustained hair growth [20]. Autoimmune disorders and systemic diseases that attack hair follicles can also impact the blood vessels surrounding the dermal papilla. Inflammation and immune cell infiltration can damage these vessels, impairing blood flow and hindering hair growth. The regression of blood vessels leads to decreased nutrient supply and hair follicle atrophy, like in androgenic or areata alopecia, contributing to hair thinning and eventual hair loss [21,22].

The dysfunction of hair cycling is seen in various hair loss disorders, such as telogen effluvium, anagen effluvium, and androgenetic alopecia [23].

Blood supply to hair follicles is primarily provided by a network of capillaries originating from dermal blood vessels. These capillaries are crucial for transporting essential nutrients and oxygen to the rapidly dividing cells within the hair bulb and follicle, fulfilling the high metabolic demands of active hair growth. The dermal papilla, situated at the base of the hair follicle, is richly vascularized, ensuring a steady supply of blood to the follicle. This dense vascular network enwraps the DP and plays a vital role in delivering essential growth factors and nutrients to the hair follicle cells [24–28].

A new generation of in vitro models has revolutionized the study of hair physiology, providing a controlled 3D microenvironment to investigate the molecular and cellular mechanisms underlying hair growth. In particular, culture systems, including hydrogels, organoids, and spheroids, have achieved a greater complexity of tissue model [29] mimicking real physiological architecture, structure, and cell phenotype [3,30] (Figure 2).

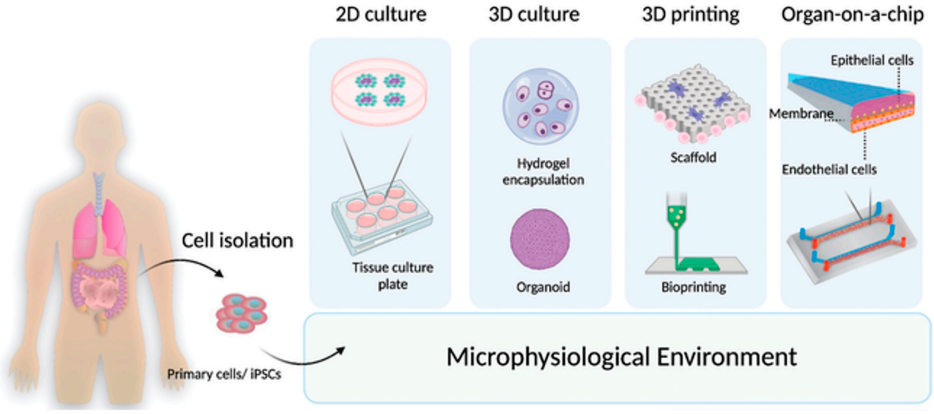


Figure 2. Schematic representation of the new generation of in vitro tissue models. From cellular isolation, microphysiological systems are developed according to advances in tissue engineering.

Moreover, these models allow for the reproduction and manipulation of the normal hair cycle through treatment with different inducers, such as TGF-β1 and FGF18, in the culture medium, enabling the study of hair follicle dynamics and regeneration in controlled experimental conditions [9,31].

Transforming Growth Factor Beta 1 (TGF-β1) and Fibroblast Growth Factor 18 (FGF-18) are critical modulators of the hair cycle, particularly in the transition between the anagen (growth), catagen (regression), and telogen (resting) phases [31–33].

Both factors exert their effects in part by regulating the expression of downstream genes involved in follicular proliferation, differentiation, and quiescence.

In the context of hair cycle regulation, *FGF7*, and *WNT5B* are key genes linked to epithelial cell proliferation and follicle maintenance. *FGF7* (also known as keratinocyte growth factor) is primarily involved in promoting epithelial cell proliferation and anagen induction [34]. *CCND1* (Cyclin D1) is a cell cycle regulator essential for G1/S phase progression and is often upregulated during active hair follicle proliferation. *WNT5B*, a non-canonical Wnt ligand, has been implicated in the regulation of hair follicle morphogenesis and cycling, often associated with promoting follicular quiescence and maintaining telogen [35]. TGF-β1 is known to induce catagen and suppress epithelial proliferation by inhibiting pro-growth signals, which may include the downregulation of *CCND1* and *FGF7*, thereby enforcing cell cycle arrest and transitioning follicles out of the anagen phase [12]. Conversely, FGF-18 has been shown to play a role in maintaining the telogen phase and preventing premature anagen entry. Its action is believed to stabilize quiescent states,

potentially by modulating *WNT5B* expression to maintain follicular dormancy, while also repressing cell cycle activators such as *CCND1*.

Among the novel 3D tissue systems developed and advances in innovative tissue engineering techniques, spheroids provide a reliable testing platform and a useful model for studying cell–cell and cell–matrix interactions, generating physiological and miniaturized tissue systems, where the cellular phenotype is preserved, and the ECM is self-produced [1,36–38].

VitroScreenORA® dermal papilla model is a scalable and reproducible 3D scaffold-free spheroid system developed by VitroScreen srl (Milan, Italy) [39–41], based on dermal papilla fibroblasts, mimicking both the physiological cycling (growth phase) and the regressive phase (catagen–telogen). Additionally, a vascularized model was created by co-culturing Hair Follicle Dermal Papilla Cells (HFDPCs) with primary dermal microvascular endothelial cells (HDMECs) (Figure 3A,B).

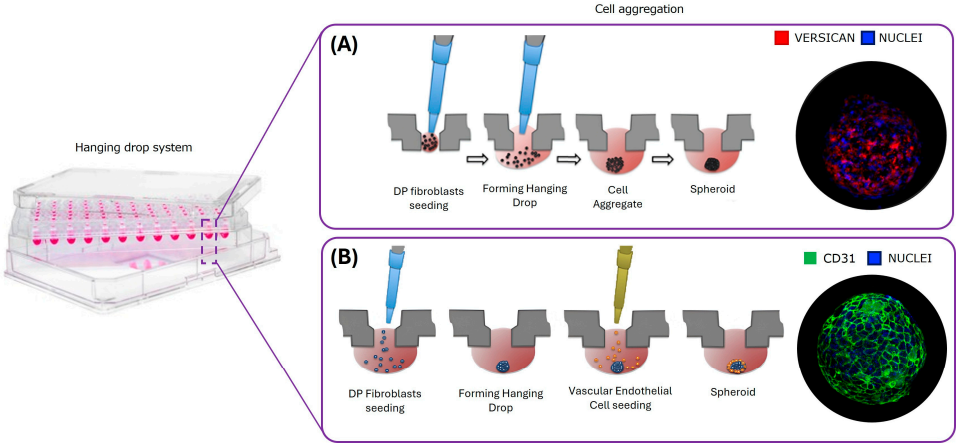


Figure 3. Graphical representation of dermal papilla spheroid development. (**A**) dermal papilla (DP) model generation. (**B**) Vascularized dermal papilla model generation (Vasc DP).

This study aims to develop and characterize the complex and responsive DP model able to establish a reliable testing platform that is useful to investigate the physiological events underlying hair cycle involution, hair stimulation, and hair loss. Firstly, the possibility of inverting the natural evolution of the DP cycle was evaluated by challenging the transition of anagen–catagen induced by the exposure to TGF- β1 10 ng/mL for 72 h. Moreover, additional exposure to FGF18 100 ng/mL for 24 h was performed to induce the catagen–telogen transition [31,42–45].

Once we defined the biological relevance of the model, a senescent and complex DP model was obtained, with the addition of vasculature, after long-term culture (11 days). In particular, the role of vasculature is crucial for supplying nutrients and oxygen to hair follicles. During intrinsic aging, the efficiency of nutrient delivery and diffusion decreases. Hair growth during the anagen phase was supported by an increased level of expression of VEGF. In senescent follicles, VEGF expression and angiogenesis are reduced, contributing to thinning and hair loss [46,47].

The biological responsiveness of the aging model to be partially restored was evaluated after treatment with a key molecule, with a known effect on the hair cycle by Minoxidil 50 µM [48–50], Doxorubicin 1 µM [51–53], and Retinol (10 ng/mL).

Minoxidil, a widely used treatment for hair loss, exerts its effects by promoting the anagen phase and enhancing hair follicle proliferation. It activates the β-catenin signaling pathway in dermal papilla cells, leading to the increased expression of growth factors such as VEGF, which supports perifollicular vascularization. Additionally, Minoxidil stimulates cell survival and proliferation within hair follicles. These mechanisms collectively contribute to prolonged anagen duration and improved hair growth outcomes [8,48–50,54–56].

Doxorubicin, a chemotherapeutic agent, adversely affects the hair cycle by inducing premature catagen development. Ex vivo studies on human hair follicles have shown that Doxorubicin treatment leads to rapid apoptosis in hair-matrix keratinocytes, resulting in the early transition from the anagen (growth) phase to the catagen (regression) phase. This process involves increased TUNEL-positive apoptotic cells and decreased proliferation markers like Ki-67 in the hair matrix, culminating in significant hair follicle dystrophy and alopecia [57].

Retinol, via its active metabolite all-trans retinoic acid (RA), plays a pivotal role in regulating hair follicle cycling. RA promotes the transition from telogen to anagen by activating hair follicle stem cells (HFSCs) through the Wnt/β-catenin signaling pathway, thereby enhancing proliferation and hair shaft elongation. In ex vivo organ cultures of androgenetic alopecia (AGA) hair follicles, treatment with RA significantly increased hair shaft growth and maintained follicles in the anagen stage, surpassing the effects observed with Minoxidil. However, elevated concentrations of RA can induce premature catagen by upregulating TGF-β2 expression in dermal papilla cells, leading to apoptosis through the Smad2/3 pathway. This biphasic effect underscores the necessity of precise RA dosing to harness its therapeutic potential in hair growth modulation [58–61].

All the DP models were deeply characterized using quantitative real-time PCR, an omics approach based on the transcriptomic defined signature, and the immunolabeling of key biomarkers on 3D whole-mount and paraffin-embedded tissues.

Thanks to their complex spatial organization, both models reproduced a miniaturized functional DP core, allowing for physiological cell orientation, polarization, and multi-compartmentalization through intercellular crosstalk. This micro-physiological system demonstrates an enhanced biological relevance for potential applications compared to ex vivo human hair follicles [43–45].

2. Materials and Methods

2.1. Cell Sources

Human Hair Follicle Dermal Papilla cells (HFDPCs) from a 51 y.o. female (Tebu-bio, Le Perray-en-Yvelines, France) were cultured in ready-to-use HFDPC Growth Medium (Tebu-bio, France), and Neonatal-dermal Human Micro-Vascular Endothelial Cells from a pool of donors (HMVEC and HMDEC) (Lonza, Italy, Innoprot, Derio, Spain, respectively) were cultured in EGMTM 2MV Basal Medium (CC-3156, Lonza, Milan, Italy).

2.2. VitroScreen ORA® 3D Scaffold-Free Spheroid Production and Treatments

At passage 5, HFDPCs were detached in a 0.05% Trypsin/EDTA solution (Lonza, Italy). Cells were counted and seeded to obtain 3D scaffold-free spheroids, for a total of 10,000 cells each. Briefly, the method employed for spheroid generation was Hanging Drop Technology, using specific culture plates (Akura® plate and Akura® V2 plate, In Sphero, Zurich, Switzerland) that allow for the development of scaffold-free spheroids using the gravity-mediated self-assembly strategy, avoiding the use of scaffolds or exogenous support.

For the vascularized model, after 40 h from HFDPC seeding, HMVEC or HDMEC at passage 6 were detached in a 0.05% Trypsin/EDTA solution (Lonza, Italy) and seeded in plates containing the spheroids. The amount of vascular endothelial cells was approximately 2000 cells per spheroid (dermal papilla fibroblasts:endothelial cells in a 4.5:1 ratio). Standard Dermal Papilla (DP) and vascularized (VASC-DP) spheroids were left on aggregation plates for a total 4 days, and then they were transferred into culture plates and cultured in standard conditions (37 °C, 5% CO_2 and 90% RH) until treatment.

The forced transition of anagen–catagen in the hair cycle was induced by exposure to TGF-β1 10 ng/mL for 72 h after complete assembly. Further exposure to FGF18 100 ng/mL brought the DP spheroids to the quiescent telogen phase.

For the senescence model, treatments with Minoxidil 50 μM, Doxorubicin 1 μM, and Retinol solution 10 ng/mL in deionized ultrapure water were performed for 11 days to modify the physiological evolution of the VASC-DP model.

2.3. Quantitative Real-Time PCR

For a first the evaluation of the key anagen genes expression after induction with TGF-β1 10 ng/mL, DP spheroids were collected in RNaqueous Lysis buffer (Thermofisher, Waltham, MA, USA) and the total RNA was extracted using a column-based RNaqueous kit (Thermofisher, Waltham, MA, USA) and was spectrophotometrically quantified. RNA quality was evaluated by electrophoresis on agarose gel. cDNA was produced by retro-transcription with High-Capacity Retrotranscriptase (Thermofisher, Waltham, MA, USA) and used for gene expression analysis by quantitative PCR in real-time using TaqMan Master Mix (Thermofisher, Waltham, MA, USA) and the following Taqman assay primers and probes: *GAPDH* Hs_99999905_m1, *CCND1* Hs_00277039_m1 and *FGF-7* Hs_00384281_m1 (Thermofisher, Waltham, MA, USA), and *WNT5B* Hs_01086864_m1 (Thermofisher, Waltham, MA, USA).

Relative Quantification analysis was performed following ΔΔCt calculation method within 35 cycles of reactions (Ct max = 35). The relative quantification (RQ) value was calculated using negative control as calibrator and the expression of GAPDH as calibrator gene for data normalization. The internal instrument level of confidence used was 95%. Signal quantification is performed in comparison with a calibrator series (in this case, a treated tissue). For data analysis, the relative quantification value (RQ) was accepted as significant when the gene was "one-fold" up (RQ > 2) or downregulated (RQ < 0.5) compared to the calibrator sample (RQ = 1).

2.4. Gene Expression Analysis Using the Nanostring nCounter® System

The NanoString platform allows for an omics approach to study specific targeted genes. The Vantage 3D™ RNA Wnt Pathways Panel CodeSet (VRXC-Wnt1-12, NanoString Technologies, Seattle, WA, USA) includes probes for 192 genes, 180 of which are related to Wnt signaling. In total, 12 housekeeping genes were included for expression normalization and quality assessment.

Biological triplicates of n = 30 pooled spheroids (for each replicate) were collected and lysed, and a total of 100 ng of isolated RNA was applied as sample input in a hybridization assay with the WNT Pathway CodeSet. Each hybridized sample was prepared on a cartridge using nCounter MAX Prep Station, and individual transcripts of the endpoint-specific biomarker signature were quantified using an nCounter MAX Digital Analyzer (NanoString Technologies, Seattle, WA, USA).

The output data, relative to the single transcript counted for each analyzed gene, were verified against the acceptance criteria before proceeding to the bio-statistical analysis.

2.5. Biostatistical Analysis

The gene expression analyses were performed in R (version 4.1.1). The quality of individual samples was assessed by considering the NanoString quality parameters, including binding density, imaging quality, the linearity of positive spike-in probes, the limit of detection, and the number of acquired counts for the positive spike-in probes. In addition, the data quality was further evaluated using techniques such as Principal Component Analysis (PCA) and relative log error plots.

Sample-specific thresholds for the limit of detection were calculated using the negative spike-in probes present in the NanoString CodeSet. The threshold was defined as the probes' mean expression values plus two standard deviations ($\mu + 2\sigma$). Genes that were consistently expressed below the limit of detection were considered undetectable in the experiment and were excluded from subsequent analyses. Genes were categorized into five different categories based on the magnitude of their expression levels across the samples. The categories were defined as not expressed (below 21 counts), low (21–100 counts), moderate (100–500 counts), high (500–2000 counts), and very high (above 2000 counts). The differential expression analysis was performed using edgeR (version 3.34.1) [51–53] *p*-values were adjusted for multiple hypothesis testing using the Benjamini & Hochberg procedure [62] based on false discovery rate (FDR). Genes with FDRs below 0.05 were considered significantly differentially expressed (and evaluated). Gene ontology (GO) enrichment analysis was performed using Fisher's exact test, using the measured genes as a background list and genes with a *p*-value from the differential expression analysis below 0.05 as the input (for assessment of overrepresentation), analyzing up- and downregulated genes separately. Principal Component Analysis (PCA) was performed on standardized (i.e., centered and scaled, $\mu = 0$ and $\sigma = 1$) expression levels for the expressed genes.

2.6. Whole-Mount Spheroid Immunolabelling

DP and VASC_DP spheroids at different timepoints, according to the different developed model (D5-D10 and D3-D7-D11), were collected for immunolabelling in 3D whole mounts. In total, 30 spheroids for each series were collected, washed in PBS 1x, and fixed in formalin-buffered solution 10% (Merck, Darmstadt, Germany) overnight at 4 °C. After tissue fixation, samples were prepared for histological clearing before incubation with the primary antibody. Samples were incubated with CD31 mouse monoclonal primary antibody (1:500, Abcam, Cambridge, UK, cat. ab9498), fibronectin rabbit polyclonal primary antibody diluted (1:400, Abcam, cat. ab2413), and versican rabbit polyclonal primary antibody (1:500, Life Technologies, Milano, Italy, cat. MA542721) overnight at 4 °C. Alexa 488 goat anti-mouse (Life Technologies, 1:600) and 555 donkey anti-rabbit (Life Technologies, 1:800) were used as secondary antibodies, while nuclei were stained with DAPI (Merck, Darmstadt, Germany, 1:2500). Stained Vascularized-DP spheroids were cleared with Visikol Histo®-M and Histodenz® (Merck, Darmstadt, Germany)-RIMS overnight at 4 °C. The acquisitions were performed using the Leica Thunder DMi8 3D Cell Imager and Leica SP8 Lightning Confocal Microscope (Leica Microsystems, Wetzlar, Germany). Z-stacks movies were acquired with a Leica sCMOS Camera (Leica Microsystems, Wetzlar, Germany) and post-processed using LASX 3.0.1 software (Leica Microsystems, Wetzlar, Germany). Z-stacks were acquired to observe the whole volumes of 3D spheroids, and expression signals were optimized using the Thunder Computational Clearing algorithm. Three more informative frames were extrapolated from the Z-stack movies for each sample.

2.7. Image Post-Processing Analysis for Vessel-like Structures Using Skeletonize (Fiji by ImageJ)

The key points of endothelial polarization and network formation on $CD31^+$ cells were evaluated using specific image analyses conducted using Skeletonize 3D, a dedicated Fiji plug-in (ImageJ-based, version 1.54 g, available at: https://fiji.sc, [63]. The software allowed us to track the branched pattern, interconnection segments, and triple-points that indicated a physiological vessel-like formation.

2.8. γH2A.X Histone as a Biomarker of Senescence in Embedded Paraffin Sections

To evaluate senescent positive nuclei for γH2A.X, 10 spheroids for each series were included in paraffin blocks. After collection, before paraffin inclusion, tissues were first fixed in 10% formalin-buffered solution (Merck, Darmstadt; Germany), pre-embedded in

3% agarose blocks (Merck, Darmstadt; Germany), in order to collect the tissues together in the hydrogel matrix, avoiding dispersion inside the paraffin block. Sections of 5 µm were prepared on tissue slides for conventional histological analysis. Each section (containing n = 10–12 pooled spheroids) was immuno-labeled for γH2A.X (primary polyclonal rabbit, 1:500, Merck, Darmstadt; Germany, cat. HPA 041189). Alexa Fluor 555 donkey anti-rabbit (Invitrogen, Waltham, MA, USA) was used a as secondary antibody, diluted 1:400 in PBS. DAPI (Merck, Darmstadt, Germany) was used for nuclei staining. The images were acquired using a LEICA DMi8 Thunder imager 3D System (Leica, Wetzlar, Germany).

2.9. Image Post-Processing Analysis for Fibronectin Fiber Orientations Using Fast Fourier Transformation (Fiji by ImageJ)

The Fast Fourier Transform (FFT) function in ImageJ (version 1.54g, available at: https://fiji.sc) enabled the analysis of fiber orientation in biological structures, providing key insights into their alignment and organization. FFT analysis provided the quantification of the directional distribution, anisotropy, and preferred orientation of FN fibers. By converting spatial patterns into frequency domain representations, this method facilitates the identification of dominant angles and structural regularities.

3. Results

3.1. TGF-β1 and FGF-18 Exposure Accelerates the Transition of the Anagen–Catagen and Catagen–Telogen Phases in the VitroScreenORA® DP Model

Hair follicles undergo cyclic transitions between anagen (growth), catagen (regression), and telogen (resting phase), orchestrated by complex molecular signaling. Among the key regulators, TGF-β1 and *FGF-7* play pivotal and distinct roles in driving follicular regression and quiescence [64,65].

In brief, TGF-β1 works as a major catagen-inducing factor, triggering the transition from anagen to catagen by promoting matrix keratinocyte apoptosis, inhibiting anagen-stimulating signals (e.g., *WNT/β-catenin*, *FGF7*), and altering dermal papilla (DP) function. Following catagen, *FGF-7* becomes a key regulator of the catagen-to-telogen transition, maintaining the follicle in a quiescent state and delaying premature anagen re-entry. By suppressing pro-anagen pathways and stabilizing keratinocyte function, *FGF-7* reinforces telogen-phase maintenance, ensuring proper hair cycle regulation [66,67].

Based on these critical considerations, the possible involvement of these key modulators of hair cycle checkpoints and the molecular signaling behind the transition of the different phases was investigated. To do this, a first attempt at an involution model was established by exposing dermal papilla spheroids to two different inducers: TGF-β1 and FGF18. Table 1 reports the specific gene signatures after 72 h of stimulation with TGF-β1 (10 ng/mL) and FGF18 100 ng/mL for an additional 24 h. Gene expression was evaluated using RT qPCR in biological triplicates for each series of pooled spheroids (n = 20/each replicate).

Table 1. Specific gene signature for the anagen–catagen and catagen–anagen transitions.

GENES	TGF-β1 10 ng/mL	FGF-18 100 ng/mL
CCND1	0.701 [1]	0.361 [1]
FGF7	0.341 [1]	0.281 [1]
WNT5B	0.971 [1]	0.601 [1]

[1] RQ study for the gene expression signature related to the forced involution model evaluated using RT qPCR. Negative control was applied as a calibrator (RQ study = 1). Upregulated genes: RQ > 2. Downregulated genes: RQ < 0.5.

Stimulation with TGF-β1 accelerated the transition from the anagen (growth) phase to the catagen (regression) phase in dermal papilla (DP) spheroids. This transition was marked

by a significant downregulation of *FGF7* expression to 0.341, indicating a reduction in proliferative signaling and confirming the initiation of the catagen phase. This observation aligns with in vivo findings, where TGF-β1 is known to induce catagen by inhibiting keratinocyte proliferation and promoting apoptosis.

The subsequent exposure of the TGF-β1-treated spheroids to FGF18 for 24 h further advanced the hair cycle into a telogen-like (resting) phase. This progression was evidenced by the significant downregulation of *CCND1* (from 0.701 to 0.361) and *WNT5B* (from 0.971 to 0.601), genes that are associated with cell cycle progression and follicular maturation, respectively. These findings are consistent with previous studies demonstrating that FGF18 maintains the telogen phase by inducing cell cycle arrest, thereby preventing premature entry into the anagen phase [31–33,68].

Collectively, these results suggest that sequential treatment with TGF-β1 and FGF18 effectively models the transition from anagen to catagen, and, subsequently, to telogen, in DP spheroids.

3.2. Transcriptomic Profiles of DP Model vs. VASC-DP Model NanoString nCounter® Technology

To deeply investigate the modulation of the specific genic signatures of the DP and VASC-DP models, cutting-edge omics technology for model characterization was applied in order to characterize the differential transcriptional profiles, focusing on the WNT pathway and its role in the hair follicle cycle.

Different levels of biostatistical analysis were applied. As a first approach, the two models were analyzed to demonstrate the relevance of the selected gene panel. Subsequently, direct comparisons were performed between conditions based on (i) the presence of vasculature and (ii) culture duration.

An omics tool was applied in biological triplicates for each series of pooled spheroids (n = 30 spheroids /each replicate) to evaluate the modulations of gene expression levels from the 180 genes analyzed. All modulated genes were separated into five discrete categories based on their expression levels (from below detection limit to very high). Although the actual thresholds and count categories are, by nature, arbitrary, this distinction is informative for the magnitude of counts. The obtained results show a normal distribution of WNT pathway genes among expression-level categories, indicating the relevance of the selected pathway for hair follicle model description. Among all investigated genes, the most expressed are involved in the assembly and organization of the extra-structural matrix (ECM) (e.g., FN1 and collagens), ECM homeostasis (MMPs and TIMP, proteases), proliferation (cyclins), and the activation of general transcription factors related to the hair follicle cycle. Moreover, a small subset of the key regulators of the hair follicle cycle was defined to assess the main transcriptomic features of the model and their evolution during the timeframe. This subset included all WNT genes: anagen-related *FGF7* and IGFI genes, proliferation-related genes, and DKKs as anagen inhibitors. Biostatistical methods were applied to capture the differences in the DP model versus the new VASC-DP model in terms of transcriptional profile.

A PCA (Principal Component Analysis) was performed to explore the main sources of variation in the defined dataset related to the differential expression profile analysis. The plot shows four different areas of sample distributions, where each series is localized in the specific quarter of the plot. Each series is represented by n = 3 biological replicates (n = 30 pooled spheroids/each replicate) in a specific quarter of plot. The highest variability (Principal Component 1, 58.8% on the x-axis) between the series is predominantly associated with the presence of the endothelial network (dark and light blue dots for the DP model vs. dark and light green dots for the VASC-DP model), indicating the direct activity of endothelial cells in the modulation of the DP gene's expression signature. A secondary

component of variability (Principal Component 2, 14.1% on the y-axis) was due to the timing of the culture: the two timepoints (D5 vs. D10) allowed for changes in transcriptional profiles, indicating the progressive evolution of the models during the timeframe of the culture (Figure 4). This data suggests that the vascular network is the primary driver of variability, followed by differences related to the culture time.

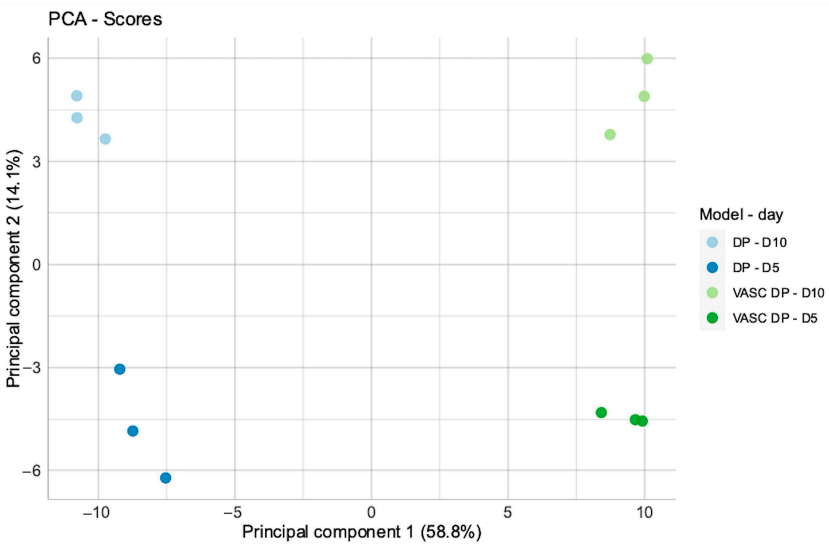


Figure 4. Principal Component Analysis (PCA). Normalized expression values for DP and DP-VASC models at day 5 and day 10 of the culture.

Differential gene expression (DGE) was performed in both models, comparing day 5 versus day 10, and the specific transcriptional signatures are reported as a heat map (Figure 5).

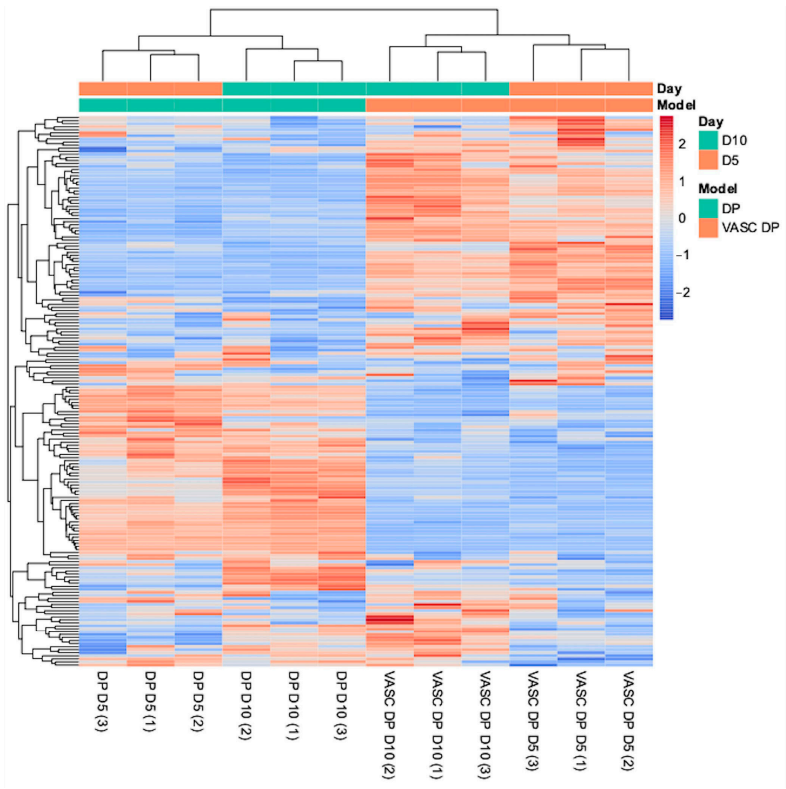


Figure 5. Differential gene expression (DGE) analysis heatmap. Data was obtained using normalized expression values for DP and DP-VASC models at day 5 and day 10 of the culture.

As reported in the DGE heatmap, different gene expression patterns between the DP and VASC-DP models were underlined during the dynamic evolution of the culture (day 5 and day 10). Considering a *p*-value threshold of 0.05, the statistically significant genes with different expressions were identified and divided into upregulated (red lines) and downregulated groups (blue lines), with different magnitudes of modulation (dark colored for high modulation, light colored for low modulation). Gene Ontology (GO) enrichment was performed on each gene group in order to identify the expression patterns related to a specific evolution of the transcriptional signature during the timeframe. Among the GO genes annotated in DP upregulation were found to be several positive regulators of proliferation, cell surface receptors for signaling, negative regulators of apoptosis, and genes related to tissue development. On the contrary, the negative regulators of the cellular process were downregulated, which correlates with DP growth.

By sorting the differentially expressed genes (DEGs), the pathway analysis comparing the DP versus the VASC-DP models was performed by the application of a Gene Set Analysis (GSA). This biostatistical analysis allowed us to summarize the effect in terms of gene expression from a selected dataset. A relative score was assigned to each annotation term (pathway): positive values indicate a global upregulation of the pathway, while negative values indicate a downregulation (Direct GSA). Using the global pathways related to WNT and comparing the DP model versus the VASC-DP model at day 10, the pathways connected to cell cycle and the specific genes related to hair cycle phases were more relevant in the DP model, while those related to adhesion and migration were more relevant in the VASC-DP model, as suggested by the Direct GSA scores shown in Table 2.

Table 2. Gene Set Analysis for DP model gene expression profile compared to VASC-DP models at D10.

Modulated Pathways	N° of DGEs	Global *	Direct **
Adhesion	6	17.9	−14.2
Cell cycle	13	16.9	5.89
Global relevance in hair follicle	32	12.3	8.46
Hair involution (catagen phase)	11	12.6	7.49
Migration	21	16.6	−7.50
Relevance for hair growth (anagen phase)	19	−9.96	5.79

* Global GSA scores are directly proportional to the magnitude of modulation. ** Direct GSA scores indicate the sign of the modulation (upregulation for positive values and downregulation for negative values).

The scores reported in the table give information on the magnitude (Global GSA) and sign (Direct GSA) of the gene's modulation: for the global scores (Global GSA), higher values correspond to the greater intensity of the modulation according to a direct proportionality. Direct scores (Direct GSA) signal the modulation: upregulation for positive values, downregulation for negative values. All positive direct scores are related to the activated pathways in the DP model, while the negative scores are related to a non-activated pathway in the DP model. A relevance in the DP model is observed for the "hair follicle cell cycle" and both anagen and catagen genes. In the VASC-DP model, the principal activated pathways are related to "adhesion and migration" as a key process in vessel formation and branching in the stromal matrix.

To further explore the omics results and associate gene expression changes with the biological relevance of angiogenesis, we conducted a direct Gene Set Analysis (GSA) using annotations related to angiogenesis and vasculogenesis (Figure 6).

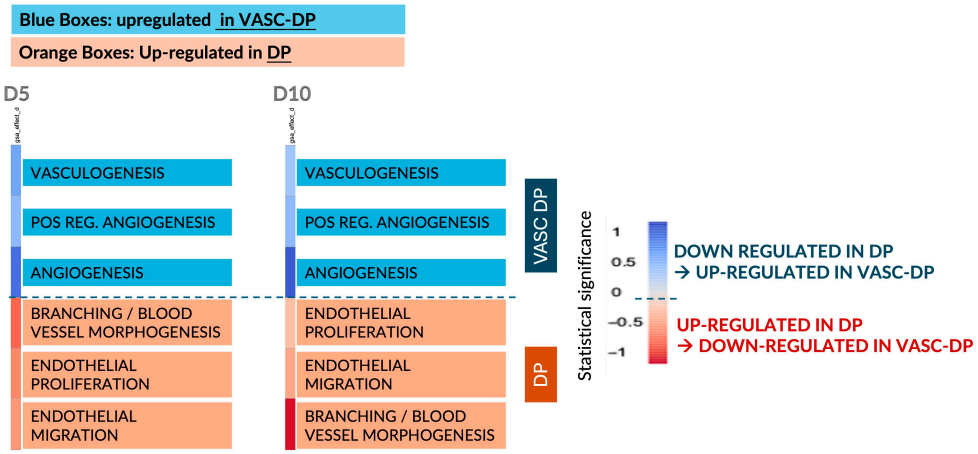


Figure 6. Summary of Gene Set Analysis (GSA) relevant for angiogenesis and vasculogenesis. The blue boxes are related to upregulated pathways in the VASC-DP model, while the red boxes underline the upregulated pathways in the DP model. The intensity of the blue and red colors is related to the magnitude of the modulation: dark colors are high modulation, light colors are low modulation.

At both D5 and D10, the pathways involved in vascular remodeling were significantly upregulated in the presence of an endothelial network (VASC-DP model), confirming the activation of pro-angiogenic mechanisms. In contrast, in the non-vascularized DP model, genes associated with endothelial proliferation and migration remained overexpressed, suggesting a constitutive pro-angiogenic signaling activity within the DP core.

The absence of endothelial cells in the DP model prevents the establishment of negative feedback regulation, leading to a sustained release of pro-angiogenic cues. Conversely, in the VASC-DP model, the presence of an endothelial network balances the angiogenic signals, creating a more physiologically relevant microenvironment. This suggests that vascularization plays a critical role in modulating DP signaling and homeostasis, which may be relevant for tissue regeneration and hair follicle cycling.

In particular, the color legend allows us to discriminate the upregulated (red) and downregulated (blue) genes, while the intensity of the color (light and dark) shows the magnitude of the up- and downregulation (dark is for an intensive modulation, light color for a mild modulation).

3.3. Evaluation of Capillary Loop Assembly Followed by CD31 and Sprouting Analysis Using Skeletonize

To confirm the presence of a functional and effective endothelial network, immunolabelling on 3D whole-mount samples for CD31 and Fibronectin (FN) to evaluate the endothelial structure and ECM architecture was performed after 10 days of culture. A very thin vessel-like structure was visible following CD31 signaling (in green), and endothelial filaments were observed in different focal planes in the 3D whole-mount structure, as shown in Figure 7 (A–C and in zoomed cropped images A'–C', white arrows).

FN fibers were visible in red in the dermal papilla core as a key structural glycoprotein at high molecular weights, supporting the dermal papilla microenvironment's stability.

To better explore the vascular network assembly and the endothelial polarization, the main key elements of vascularization (branches, junctions, and triple-points), were followed and quantified on $CD31^{+}$-Z-stacks using Skeletonize 3D, a Fiji plugin.

The Skeletonize algorithm was applied to the images to evaluate the number of branches, junctions, and triple-points, as reported in Table 3. The patterned image (Figure 7D,E) shows the endothelial network's organization.

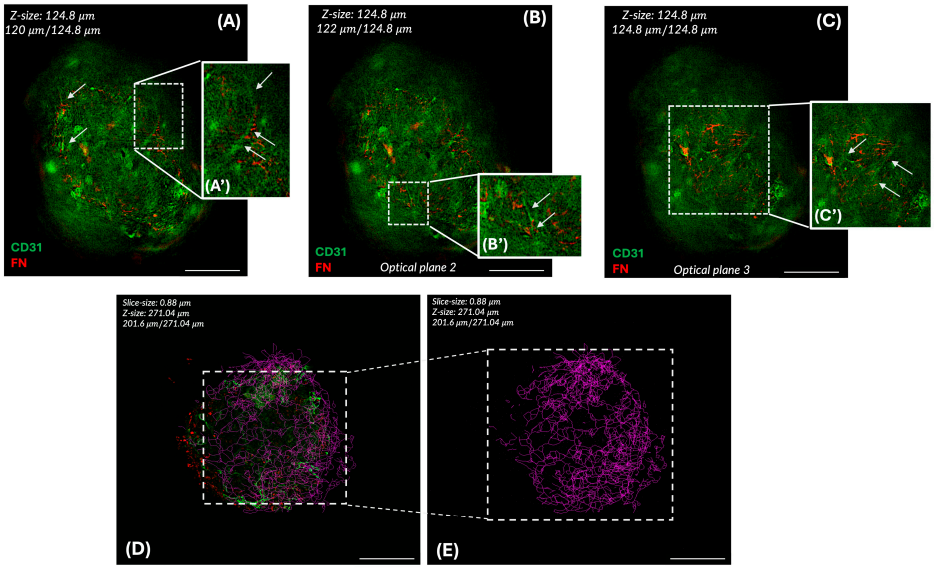


Figure 7. Immunofluorescence for CD31 and FN. Different optical planes are presented (**A**–**C**) to evaluate endothelial polarization and sprouting. Cropped zoomed images underline the early endothelial network (white arrows) inside the 3D structure of the VASC-DP model (**A′**–**C′**). The endothelial network is labeled using Skeletonize 3D, a Fiji plugin (**D**,**E**) at D7. The green pattern (**D**) indicates the end-point voxels, the terminal points of the skeleton, as segment ends. The magenta pattern (**E**) indicates the junction voxels, being multiple segments of the skeleton that are connected. Scale bar = 50 µm.

Table 3. Characterization of the vascular structure.

N° Branches (in Mean)	N° Junctions (in Mean)	N° Triple points (in Mean)
3744	1591	1153

Branches, junctions, and triple-points are related to the grade of the new vessels' formation and their physiological vascularization.

The branched pattern with clear zones and interconnections segments, the peripheral small segments, and the presence of triple-points suggests a vessel-like network close to the physiological capillary loop embedding the DP core, with dynamic sprouting events confirmed using VASC model morphology.

3.4. Physiological Senescence of the VASC-DP Model During the Time of Culture, and the Effect of Different Treatments on the Aged Dermal Papilla Profile

Once we defined the main features for a more physiological in vitro dermal papilla compartment, the effect of time on the structure was evaluated to study the natural chronological aging responsible for hair cycle regression and hair loss (together with the acceleration of the anagen–catagen and catagen–telogen transitions) (Figure 8).

Thanks to its high specificity, CD31 was used as a tracker to follow the endothelial evolution during the timeframe. As observed in Figure 8A,B, at D0 (immediately after the model assembly), the endothelial network was visible as an external envelope embedding the dermal papilla's core. After 7 days (D7), the endothelial network modified its configuration, reaching the highest polarization and sprouting of the endothelial network (Figure 8C,D). Histological investigations confirmed a regression of DP organization and vascular structure after 11 days of culture (Figure 9A), suggesting that a possible physiological aging occurred in long-term culture, mirroring a senescent DP compartment. The different effects of specific treatments were tested on the senescent VASC-DP, aiming to observe the possible restoration of the structure and niche organization followed by IF key biomarkers (Figure 9).

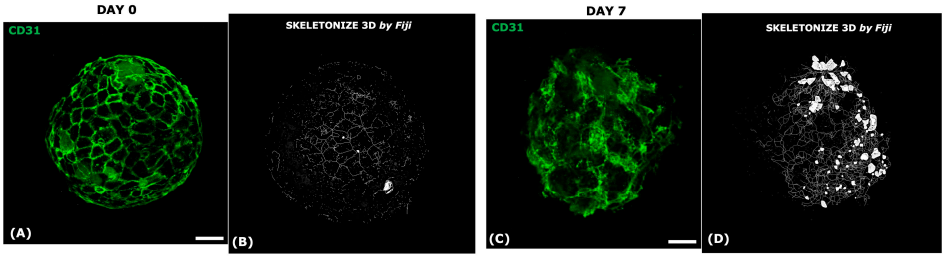


Figure 8. Immunofluorescence for CD31 to follow the evolution of the endothelial network at D0 and D7. The endothelial network at D0 (**A**) and D7 (**C**); Skeletonize analysis (**B**,**D**).

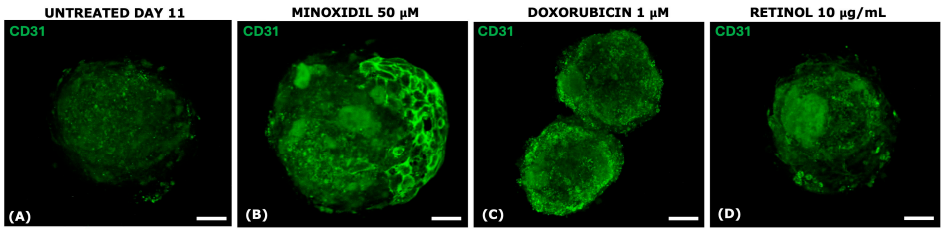


Figure 9. Immunofluorescence for CD31 on senescent treated VASC-DP spheroids at D11. The effect of different treatments on the endothelial network at D11 was observed using CD31-IF: exposure to minoxidil (**B**), doxorubicin (**C**), and Retinol (**D**) compared to untreated senescent spheroids (**A**). Scale bar = 50 µm.

After 11 days of culture, untreated VASC-DP samples showed a progressive and spontaneous regression, with a loss of defined vascular structure shown with a reduction in the endothelial cell CD31$^+$ (Figure 9A). Long-term exposure to Minoxidil 50 µM led to a partial restoration of the endothelial network, showing a recovery of the net structure around the spheroids (Figure 9B). As expected, Doxorubicin severely damaged VASC-DP tissues, showing a dotted green signal for CD31 (indicating a cellular membrane impairment) and the loss of tissue architecture. Exposure to Retinol solution led to a slight preservation of the endothelial polarization, suggesting a possible effect on the progression of tissue aging that occurred during the time of culture.

To deeply investigate the direct effect of treatments on senescence, γH2A.X histone was evaluated as a specific key biomarker involved in the DNA damage that occurred during tissue aging (Figure 10). In particular, γH2A.X is an H2A histone variant, synthesized and then phosphorylated to tag the DSBs (Double Strand Breaks) that need to be repaired. The presence of γH2A.X$^+$ cells confirmed the presence of cellular damage related to the senescence [69,70].

The physiological senescence of the VASC-DP models was confirmed by the positivity of cells for γH2A.X signals (Figure 10, red signal).

In particular, under certain stress conditions, chromatin can reorganize, altering the typical γ-H2AX distribution; DNA damage loci could appear diffused and not localized in distinct foci. Moreover, some DNA repair mechanisms may influence the spatial organization of γ-H2AX [69,70].

In the untreated series, after 11 days, γH2A.X expression was high and globally diffused in the spheroid's core. Exposure to Minoxidil (Figure 10B,F) led to a reduction in red-positive cells, showing a preservation of the DNA damage that occurred during the senescence. The positive effect of Retinol (Figure 10C,G) in preserving global cell senescence was visible (if compared to untreated series, cultured for 11 days), but less intense than Minoxidil activity. On the contrary, as expected, Doxorubicin (Figure 10D,H) caused global cellular damage, showing a diffused global dotted-red signal, with a loss of DAPI nuclear signal (in blue), indicating a severe degradation in nuclear structure and a severe genomic

impairment. The fragmented, linear red signal could suggest a possible association of gH2A.X with the nuclear membrane or a possible recruitment near the nuclear lamina or nuclear pores [71,72].

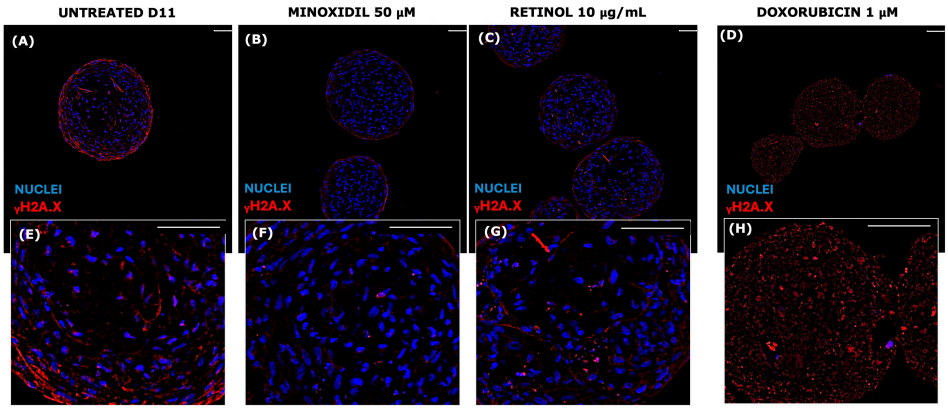


Figure 10. Immunofluorescence for γH2A.X on paraffin sections of senescent VASC-DP spheroids at D11. The senescent profile was confirmed after 11 days of culture in untreated series, with positive red cells and blue nuclei ((**A**,**E**) in a greater magnification). γH2A.X profiles of minoxidil (**B**,**F**), retinol (**C**,**G**), and doxorubicin (**D**,**H**) series are compared to untreated samples. Scale bar = 50 µm.

The structural configuration and the effect on the whole architecture were evaluated by monitoring FN deposition and its orientation on 3D whole-mount samples.

FN is an extracellular matrix glycoprotein providing a supportive scaffold in the hair follicle niche, mediating cell adhesion and migration. Indeed, in the dermal papilla stroma, it works as a bridge between cells and ECM, driving a cell-mediated traction, an increase in stromal architecture complexity, matrix stiffness, chemical gradient, and biophysical cues. The topographical patterns given by the ECM structure and organization provided guidance for FN orientation (Figure 11).

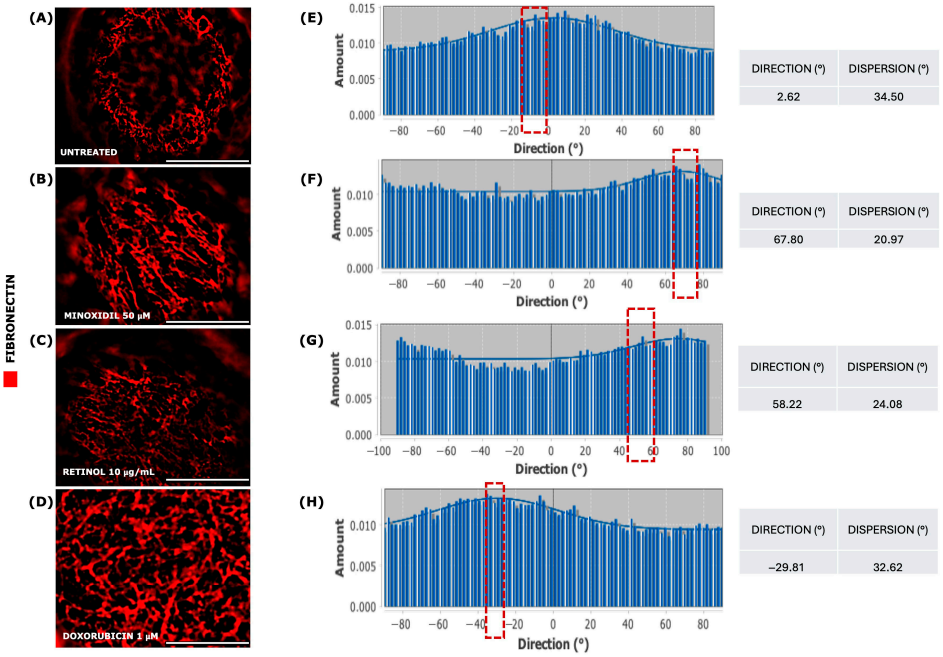


Figure 11. Immunofluorescence for FN on 3D whole-mount senescent VASC-DP spheroids at D11. FN red fibers were observed in Minoxidil (**B**), Retinol (**C**), and Doxorubicin (**D**) compared to untreated unexposed series (**A**). Fiber orientation and alignment (red dotted box) were evaluated using FFT (ImageJ plugin, version 2.16.0/1.54p) on selected focal planes from each Z-stack (**E**–**H**). Scale bar = 50 µm.

Aligned fibronectin fibers provide structural support and guide cell behavior in terms of cell migration, tissue remodeling, and mechano-sensing [42,73–75]. The specific orientation of fibers was measured by applying the FFT (Fast Fourier Transform) algorithm. Exposure to Minoxidil and, for a lesser extent, to Retinol solution led to a preferential alignment of endogenous fibronectin fibers according to a specific and optimal orientation, confirmed by the lowest degree of dispersion (20.97° and 24.08°, respectively; Figure 11B,C) even compared to the negative control, where fibers appeared as randomly distributed (34.50°, Figure 11A). Doxorubicin has determined a fibronectin network disassembly with a random distribution of fragmented fibers, a low degree of dispersion, similar to untreated series (32.62°, Figure 11D).

Taken together, these data suggested that Minoxidil and Retinol solution exposure had a greater impact on FN orientation and microstructural niche organization.

4. Discussion

An innovative senescent hair follicle model was developed as a 3D spheroid combining a dermal papilla stromal compartment with an endothelial network. This in vitro study establishes a regression/senescence model to better investigate the signaling mechanisms and molecular pathways underlying progressive hair regression, which culminate in permanent hair loss. Hair cycle regression was mimicked using two different models: a forced involution model, and a physiological senescent model.

The efficacy of molecules with known roles in hair follicle biology was tested to confirm the responsiveness of the tissues to specific treatments in counteracting the natural regression of the hair follicle. The forced involution model was partially simulated by exposure to critical molecular inducers: TGF-β1 as an anagen–catagen transition accelerator, and FGF-18 as a catagen–telogen transition modulator. Treatment with TGF-β1 led to reduced dermal papilla proliferation and hair elongation arrest. Additional treatment with FGF-18 accelerated the subsequent transition to the quiescent telogen phase. The downregulation of critical anagen genes belonging to the WNT pathway confirmed the regression profile, suggesting possible responsiveness to anagen stimulators [76,77]. Indeed, the combined negative modulation of *FGF7*, *WNT5B*, and *CCND1* confirmed the direct involvement of these genes in the proliferative steps of the dermal papilla niche [69,78–81].

To establish a more complex dermal papilla model, an endothelial network was added to the DP core, mimicking the physiological capillary loop [70]. The presence of a defined microvasculature increased the biological relevance and physiological accuracy of the in vitro model. Cutting-edge omics technology was applied to evaluate the transcriptional profile (compared to an avascular transcriptional profile), focusing on the *WNT* pathway and its role in the hair follicle cycle.

Advanced biostatistical analysis for data dimensionality reduction [82] showed that the *WNT* pathway is differentially modulated in both DP and VASC-DP, underlining the contribution of endothelial cells and the influence of culture time. A comparison between differentially expressed genes was performed using DGE analysis followed by enrichment analysis techniques such as Gene Ontology (GO). GO enrichment analysis is commonly used for interpreting high-throughput molecular data and generating hypotheses about the underlying biological mechanisms [83]. This approach allowed for the detection of pathways within the WNT cascade that were positively or negatively modulated over time, assessing which signaling pathways were mostly involved in the DP and VASC-DP models.

Morphological analysis of VASC-DP spheroids confirmed the establishment of an endothelial network of vessel-like components. The application of the Skeletonize tool in post-processing analysis confirmed that the capillary loop was organized as a protective envelope that is able to embed and nourish the stromal compartment. Branches with

several junctions and triple-points suggest a dynamically growing physiological vasculature assembly, conferring greater biological relevance. The presence of a stromal compartment provides specific key signaling for endothelial orientation and polarization, leading to endothelial sprouting and the generation of new vessel-like structures [70,84]. Furthermore, the presence of an endothelial network increases the complexity of the model and enhances physiological assessment, as the capillary loop extends DP niche survival and regeneration, preserving the anagen phase.

A senescent model of vascularized dermal papilla spheroids was established by extending the culture for 11 days. The aged VASC-DP model mirrored the physiological intrinsic senescence, showing a compromission of the vascular structure [85,86]. DNA integrity, and FN structure [87]; the endothelial envelope appeared missing (spot-like signal for CD31) with the loss of cellular integrity. Positive cells for H2A.X confirmed the presence of DSBs during the natural aging [88].

Selected treatments were evaluated for their ability to restore the aged profile in terms of vasculature structure, DNA damage, and structural organization.

Minoxidil is known to be a stimulator of the hair cycle. Strong evidence confirms its direct effect on promoting hair growth via the stimulation of DP and epithelial cells through the activation of the WNT-mediated β-catenin pathway [49,65,89–91]. Exposure to Minoxidil (50 μM) for 11 days partially restored the vascular envelope, which was missing in aged VASC-DP during long-term culture. The activation of DP's core metabolism induced by Minoxidil was observed by the reduction in DSB-positive cells, suggesting the preservation of cellular integrity. A positive effect was also observed in structural and architectural terms, showing an impact on fibronectin fiber orientation. The alignment of FN fibers confirmed an increase in ECM complexity, providing physical signals for cell-traction activity and cell–matrix crosstalk.

In parallel, aged VASC-DP spheroids were further challenged with Doxorubicin (1 μM), a commonly used chemotherapy drug known to negatively affect hair growth and cause hair loss [54,55]. As expected, exposure to Doxorubicin led to severe DP regression with widespread cellular damage and the loss of an organized vascular network, confirming the model's responsiveness.

Surprisingly, Retinol (10 μg/mL) seemed to slightly act on chronological cellular damage by reducing H2A.X-positive cells, suggesting its mild efficacy in counteracting progressive tissue impairment due to senescence [92]. In addition to this interesting effect, Retinol also stimulated FN fiber orientation, giving the ECM a specific physiological topography and ensuring the physiological architecture of the DP niche [93,94].

The development of a micro-physiological dermal papilla (DP) model using hanging drop technology represents a significant advancement in replicating the complexity of human hair follicle biology in vitro. Unlike traditional 2D cultures or simplified spheroid systems, this 3D model successfully mimics the structural organization and functional behavior of native DP tissue, including its role in regulating the hair growth cycle. In particular, it captures key physiological transitions—from the anagen and catagen to telogen phases—either through spontaneous aging or experimentally induced involution, offering a rare opportunity to study dynamic hair follicle processes under controlled conditions.

A particularly innovative aspect of this model is the incorporation of a vascular-like endothelial envelope, mirroring the native microenvironment of the hair bulb. The resulting increase in complexity facilitates more physiologically relevant cell–matrix and cell–cell interactions, which are crucial for modeling the niche dependent behavior of DP cells. The model's responsiveness to pharmacological interventions further supports its potential as a predictive platform for drug screening. Treatments targeting aging-related pathways demonstrate not only their protective effects, but also the partial reversal of tissue

senescence markers, indicating a level of plasticity in the DP microenvironment that could be exploited therapeutically. These findings are consistent with recent studies highlighting the rejuvenating potential of targeted growth factors and small molecules in aged dermal papilla cells [12,68].

Future work should focus on integrating follicular keratinocytes to more accurately reproduce the hair bulb niche, which could further enhance the model's physiological fidelity.

Overall, this 3D micro-physiological system represents a promising tool not only for understanding human hair biology, but also for accelerating the development of novel therapeutic strategies against alopecia and hair aging.

5. Conclusions

The primary aim of this study was to develop a novel in vitro model of the dermal papilla (DP) able to recapitulate the main physiological processes involved in hair growth and regression. Hanging drop technology successfully generated micro-physiological DP spheroids that incorporated a vascular component, enhancing the biological relevance of the model. To investigate the mechanisms underlying hair cycle regulation, VitroScreenORA® implemented two experimental paradigms: a forced involution model and a chronological aging model. The forced involution model accelerated the transition from the anagen to catagen phase by exposing the spheroids to specific growth factors (TGF-β1 10 ng/mL). The chronological aging model mimicked the natural progression of hair follicle aging by culturing the spheroids over an extended period. The results demonstrate that the in vitro DP model faithfully recapitulates the key aspects of hair follicle biology, including cell proliferation, differentiation, and apoptosis. The vascularization of the spheroids significantly impacted the behavior of the DP cells, suggesting the crucial role of the microenvironment in regulating hair growth. Furthermore, the treatment of senescent spheroids with specific compounds, such as Minoxidil (50 μM) and Retinol (10 μg/mL), resulted in the partial restoration of hair follicle structure and function, highlighting the potential of this model for drug discovery and development.

The VitroScreen® DP models presented in this study provide a valuable tool for investigating the molecular mechanisms underlying hair growth and regression, confirming themselves to be a stable and reliable platform for the development of novel therapies for hair loss and other hair-related disorders.

6. Patents

To develop the VitroScreenORA® VASC-DP model, a sequential co-culture was performed according to the VitroScreen internal procedure described in the international publication WO/2019/092667 A1 (patents.google.com/patent/WO2019092667A1/en).

Author Contributions: Conceptualization, F.R.; methodology, F.R., G.M. and C.G.; software, G.M. and F.R.; validation, F.R., G.M. and C.G.; formal analysis, F.R., G.M. and C.G.; data curation, F.R. and G.M.; writing—original draft preparation, F.R. and G.M.; writing—review and editing, F.R. and G.M.; supervision and project administration, F.R. All authors have read and agreed to the published version of the manuscript.

Funding: This research received no external funding.

Institutional Review Board Statement: Not applicable.

Informed Consent Statement: Not applicable.

Data Availability Statement: Dataset available on request from the authors; the raw data supporting the conclusions of this article will be made available by the authors on request.

Acknowledgments: We would like to express our sincere gratitude to all those who contributed to the successful completion of this study. We are deeply grateful to our colleagues at IFOM (Istituto Fondazione Oncologia Molecolare ETS) for their invaluable assistance and technical support for some image acquisitions, and to Robin Gradin for his technical support for biostatistical analyses and results interpretation of NanoString nCounter® results.

Conflicts of Interest: VitroScreenORA® is a registered trademark of VitroScreen srl. The authors declare there are no conflicts of interest related to this work.

References

1. Higgins, C.A.; Chen, J.C.; Cerise, J.E.; Jahoda, C.A.B.; Christiano, A.M. Microenvironmental reprogramming by three-dimensional culture enables dermal papilla cells to induce de novo human hair-follicle growth. *Proc. Natl. Acad. Sci. USA* **2013**, *110*, 19679–19688. [CrossRef]
2. Havlickova, B.; Bíró, T.; Mescalchin, A.; Tschirschmann, M.; Mollenkopf, H.; Bettermann, A.; Pertile, P.; Lauster, R.; Bodó, E.; Paus, R. A Human Folliculoid Microsphere Assay for Exploring Epithelial–Mesenchymal Interactions in the Human Hair Follicle. *J. Investig. Dermatol.* **2009**, *129*, 972–983. [CrossRef]
3. Kang, D.; Liu, Z.; Qian, C.; Huang, J.; Zhou, Y.; Mao, X.; Qu, Q.; Liu, B.; Wang, J.; Hu, Z.; et al. 3D bioprinting of a gelatin-alginate hydrogel for tissue-engineered hair follicle regeneration. *Acta Biomater.* **2023**, *165*, 19–30. [CrossRef] [PubMed]
4. Ohyama, M.; Kobayashi, T.; Sasaki, T.; Shimizu, A.; Amagai, M. Restoration of the intrinsic properties of human dermal papilla in vitro. *J. Cell Sci.* **2012**, *125*, 4114–4125. [CrossRef] [PubMed]
5. Saxena, N.; Mok, K.; Rendl, M. An updated classification of hair follicle morphogenesis. *Exp. Dermatol.* **2019**, *28*, 332–344. [CrossRef] [PubMed]
6. Sennett, R.; Rendl, M. Mesenchymal–epithelial interactions during hair follicle morphogenesis and cycling. *Semin. Cell Dev. Biol.* **2012**, *23*, 917–927. [CrossRef] [PubMed]
7. Driskell, R.R.; Clavel, C.; Rendl, M.; Watt, F.M. Hair follicle dermal papilla cells at a glance. *J. Cell Sci.* **2011**, *124*, 1179–1182. [CrossRef]
8. Botchkarev, V.A. Molecular Mechanisms of Chemotherapy-Induced Hair Loss. *J. Investig. Dermatol. Symp. Proc.* **2003**, *8*, 72–75. [CrossRef]
9. Paus, R.; Foitzik, K. In search of the "hair cycle clock": A guided tour. *Differentiation* **2004**, *72*, 489–511. [CrossRef]
10. Oh, J.W.; Kloepper, J.; Langan, E.A.; Kim, Y.; Yeo, J.; Kim, M.J.; Hsi, T.-C.; Rose, C.; Yoon, G.S.; Lee, S.-J.; et al. A Guide to Studying Human Hair Follicle Cycling In Vivo. *J. Investig. Dermatol.* **2016**, *136*, 34–44. [CrossRef]
11. Zhang, H.-L.; Qiu, X.-X.; Liao, X.-H. Dermal Papilla Cells: From Basic Research to Translational Applications. *Biology* **2024**, *13*, 842. [CrossRef] [PubMed]
12. Plikus, M.V. New Activators and Inhibitors in the Hair Cycle Clock: Targeting Stem Cells' State of Competence. *J. Investig. Dermatol.* **2012**, *132*, 1321–1324. [CrossRef]
13. Chi, W.; Wu, E.; Morgan, B.A. Dermal papilla cell number specifies hair size, shape and cycling and its reduction causes follicular decline. *Development* **2013**, *140*, 1676–1683. [CrossRef]
14. Elliott, K.; Messenger, A.G.; Stephenson, T.J. Differences in Hair Follicle Dermal Papilla Volume are Due to Extracellular Matrix Volume and Cell Number: Implications for the Control of Hair Follicle Size and Androgen Responses. *J. Investig. Dermatol.* **1999**, *113*, 873–877. [CrossRef]
15. Enshell-Seijffers, D.; Lindon, C.; Wu, E.; Taketo, M.M.; Morgan, B.A. β-Catenin activity in the dermal papilla of the hair follicle regulates pigment-type switching. *Proc. Natl. Acad. Sci. USA* **2010**, *107*, 21564–21569. [CrossRef]
16. Schneider, M.R.; Schmidt-Ullrich, R.; Paus, R. The Hair Follicle as a Dynamic Miniorgan. *Curr. Biol.* **2009**, *19*, R132–R142. [CrossRef] [PubMed]
17. Garza, L. Developmental Biology of the Skin. In *Fitzpatrick's Dermatology*, 9th ed.; Kang, S., Amagai, M., Bruckner, A.L., Enk, A.H., Margolis, D.J., McMichael, A.J., Orringer, J.S., Eds.; McGraw-Hill Education: New York, NY, USA, 2019.
18. Lim, J.; Ng, K.J.; Clavel, C. Dermal papilla regulation of hair growth and pigmentation. In *Advances in Stem Cells and their Niches*; Elsevier: Amsterdam, The Netherlands, 2019; Volume 3, pp. 115–138.
19. Millar, S.E. Molecular Mechanisms Regulating Hair Follicle Development. *J. Investig. Dermatol.* **2002**, *118*, 216–225. [CrossRef] [PubMed]
20. Li, K.N.; Jain, P.; He, C.H.; Eun, F.C.; Kang, S.; Tumbar, T. Skin vasculature and hair follicle cross-talking associated with stem cell activation and tissue homeostasis. *eLife* **2019**, *8*, e45977. [CrossRef]
21. Deng, Z.; Chen, M.; Liu, F.; Wang, Y.; Xu, S.; Sha, K.; Peng, Q.; Wu, Z.; Xiao, W.; Liu, T.; et al. Androgen Receptor–Mediated Paracrine Signaling Induces Regression of Blood Vessels in the Dermal Papilla in Androgenetic Alopecia. *J. Investig. Dermatol.* **2022**, *142*, 2088–2099.e9. [CrossRef]

22. Leirós, G.J.; Kusinsky, A.G.; Drago, H.; Bossi, S.; Sturla, F.; Castellanos, M.L.; Stella, I.Y.; Balañá, M.E. Dermal Papilla Cells Improve the Wound Healing Process and Generate Hair Bud-Like Structures in Grafted Skin Substitutes Using Hair Follicle Stem Cells. *Stem Cells Transl. Med.* **2014**, *3*, 1209–1219. [CrossRef]
23. Paus, R.; Cotsarelis, G. The Biology of Hair Follicles. *N. Engl. J. Med.* **1999**, *341*, 491–497. [CrossRef]
24. Murphrey, M.B.; Agarwal, S.; Zito, P.M. Anatomy, Hair. In *StatPearls*; StatPearls Publishing: Treasure Island, FL, USA, 2024.
25. Yoshida, Y.; Soma, T.; Kishimoto, J. Characterization of human dermal sheath cells reveals CD36-expressing perivascular cells associated with capillary blood vessel formation in hair follicles. *Biochem. Biophys. Res. Commun.* **2019**, *516*, 945–950. [CrossRef]
26. Inaba, M.; Inaba, Y. Blood Vessel System in Hair Follicles. In *Androgenetic Alopecia: Modern Concepts of Pathogenesis and Treatment*; Inaba, M., Inaba, Y., Eds.; Springer: Tokyo, Japan, 1996; pp. 39–44.
27. Woodfin, A.; Voisin, M.-B.; Nourshargh, S. PECAM-1: A Multi-Functional Molecule in Inflammation and Vascular Biology. *ATVB* **2007**, *27*, 2514–2523. [CrossRef] [PubMed]
28. Lertkiatmongkol, P.; Liao, D.; Mei, H.; Hu, Y.; Newman, P.J. Endothelial functions of platelet/endothelial cell adhesion molecule-1 (CD31). *Curr. Opin. Hematol.* **2016**, *23*, 253–259. [CrossRef] [PubMed]
29. Kavand, H.; Nasiri, R.; Herland, A. Advanced Materials and Sensors for Microphysiological Systems: Focus on Electronic and Electrooptical Interfaces. *Adv. Mater.* **2022**, *34*, 2107876. [CrossRef] [PubMed]
30. Zheng, W.; Xu, C.-H. Innovative Approaches and Advances for Hair Follicle Regeneration. *ACS Biomater. Sci. Eng.* **2023**, *9*, 2251–2276. [CrossRef]
31. Kimura-Ueki, M.; Oda, Y.; Oki, J.; Komi-Kuramochi, A.; Honda, E.; Asada, M.; Suzuki, M.; Imamura, T. Hair Cycle Resting Phase Is Regulated by Cyclic Epithelial FGF18 Signaling. *J. Investig. Dermatol.* **2012**, *132*, 1338–1345. [CrossRef]
32. Mori, O.; Hachisuka, H.; Sasai, Y. Effects of Transforming Growth Factor β1 in the Hair Cycle. *J. Dermatol.* **1996**, *23*, 89–94. [CrossRef]
33. Kawano, M.; Umeda, S.; Yasuda, T.; Fujita, M.; Ishikawa, A.; Imamura, T.; Imai, T.; Nakayama, F. FGF18 signaling in the hair cycle resting phase determines radioresistance of hair follicles by arresting hair cycling. *Adv. Radiat. Oncol.* **2016**, *1*, 170–181. [CrossRef]
34. Rosenquist, T.A.; Martin, G.R. Fibroblast growth factor signalling in the hair growth cycle: Expression of the fibroblast growth factor receptor and ligand genes in the murine hair follicle. *Dev. Dyn.* **1996**, *205*, 379–386. [CrossRef]
35. Kandyba, E.; Kobielak, K. Wnt7b Is an Important Intrinsic Regulator of Hair Follicle Stem Cell Homeostasis and Hair Follicle Cycling. *Stem Cells* **2014**, *32*, 886–901. [CrossRef] [PubMed]
36. Bejaoui, M.; Oliva, A.K.; Ke, M.S.; Ferdousi, F.; Isoda, H. 3D Spheroid Human Dermal Papilla Cell as an Effective Model for the Screening of Hair Growth Promoting Compounds: Examples of Minoxidil and 3,4,5-Tri-O-caffeoylquinic acid (TCQA). *Cells* **2022**, *11*, 2093. [CrossRef]
37. Bejaoui, M.; Oliva, A.K.; Ke, M.S.; Ferdousi, F.; Isoda, H. Establishment of 3D Spheroid Human Dermal Papilla Cells as an Effective Model for Hair Growth Screening Compounds Compared with the 2D System: An Example of Minoxidil and 3,4,5-Tri-O-caffeoylquinic acid (TCQA). 2021; *in press*. [CrossRef]
38. Lin, B.; Miao, Y.; Wang, J.; Fan, Z.; Du, L.; Su, Y.; Liu, B.; Hu, Z.; Xing, M. Surface Tension Guided Hanging-Drop: Producing Controllable 3D Spheroid of High-Passaged Human Dermal Papilla Cells and Forming Inductive Microtissues for Hair-Follicle Regeneration. *ACS Appl. Mater. Interfaces* **2016**, *8*, 5906–5916. [CrossRef]
39. Laura, C.; Elisa, C.; Marisa, M.; Francesco, C. 3D Scaffold Free Micro-Dermis Model: An Innovative Tool to Explore Dermal Matrix Remodeling. Available online: https://www.vitroscreen.com/wp-content/uploads/2024/04/13_2019-POSTER-MICRODERMIS_IFSCC.pdf (accessed on 30 June 2025).
40. Aiello, G.; Rescigno, F.; Meloni, M.; Baron, G.; Aldini, G.; Carini, M.; D'Amato, A. Oxidative Stress Modulation by Carnosine in Scaffold Free Human Dermis Spheroids Model: A Proteomic Study. *IJMS* **2022**, *23*, 1468. [CrossRef]
41. Aiello, G.; Rescigno, F.; Meloni, M.; Zoanni, B.; Aldini, G.; Carini, M.; D'Amato, A. The Effect of Carnosine on UVA-Induced Changes in Intracellular Signaling of Human Skin Fibroblast Spheroids. *Antioxidants* **2023**, *12*, 300. [CrossRef] [PubMed]
42. Tan, C.T.; Lim, C.Y.; Lay, K. Modelling Human Hair Follicles—Lessons from Animal Models and Beyond. *Biology* **2024**, *13*, 312. [CrossRef] [PubMed]
43. Elisa, C.; Meloni, M.; De Servi, B. Hair Follicle Bulb Developed as 3D Scaffold-Free Microtissue. *J. Investig. Dermatol.* **2017**. Available online: https://tressless.com/research/3d-scaffold-free-hair-follicle-microtissue-development-l8xM (accessed on 30 June 2025).
44. Meloni, M.; Carriero, F.; Guiducci, C.; Rescigno, F. 722 Dermal papilla: 3D scaffold free spheroid self-renewing mini-organ. *J. Investig. Dermatol.* **2024**, *144*, S126. [CrossRef]
45. Baratto, G.; Caviola, E.; Meloni, M.; Lionetti, N.; Bonfigli, A.; Sironi, M.; Pieraccini, S.; Oliver, M.; Coderch, L.; Rigano, L. Hair Strengthening Evaluation of Anisotropic Osmolite Solutions (Inositol + Arginine): Cross-Talk between Dermal Papilla Fibroblast and Keratinocytes of the Outer Root Sheath Using a μHair Follicle 3D Model. *Cosmetics* **2018**, *5*, 56. [CrossRef]
46. Yano, K.; Brown, L.F.; Detmar, M. Control of hair growth and follicle size by VEGF-mediated angiogenesis. *J. Clin. Invest.* **2001**, *107*, 409–417. [CrossRef]

47. Morgan, B.A. Upending the hair follicle. *Nat. Genet.* **2006**, *38*, 273–274. [CrossRef] [PubMed]
48. Han, J.H.; Kwon, O.S.; Chung, J.H.; Cho, K.H.; Eun, H.C.; Kim, K.H. Effect of minoxidil on proliferation and apoptosis in dermal papilla cells of human hair follicle. *J. Dermatol. Sci.* **2004**, *34*, 91–98. [CrossRef]
49. Marubayashi, A.; Nakaya, Y.; Fukui, K.; Li, M.; Arase, S. Minoxidil-Induced Hair Growth is Mediated by Adenosine in Cultured Dermal Papilla Cells: Possible Involvement of Sulfonylurea Receptor 2B as a Target of Minoxidil. *J. Investig. Dermatol.* **2001**, *117*, 1594–1600. [CrossRef] [PubMed]
50. You, J.; Jang, Y.; Sim, J.; Ryu, D.; Cho, E.; Park, D.; Jung, E. Anti-Hair Loss Effect of Veratric Acid on Dermal Papilla Cells. *IJMS* **2025**, *26*, 2240. [CrossRef] [PubMed]
51. McCarthy, D.J.; Chen, Y.; Smyth, G.K. Differential expression analysis of multifactor RNA-Seq experiments with respect to biological variation. *Nucleic Acids Res.* **2012**, *40*, 4288–4297. [CrossRef]
52. Gandolfo, L.C.; Speed, T.P. RLE plots: Visualizing unwanted variation in high dimensional data. *PLoS ONE* **2018**, *13*, e0191629. [CrossRef]
53. Robinson, M.D.; McCarthy, D.J.; Smyth, G.K. edgeR: A Bioconductor package for differential expression analysis of digital gene expression data. *Bioinformatics* **2010**, *26*, 139–140. [CrossRef] [PubMed]
54. Amoh, Y.; Li, L.; Yang, M.; Jiang, P.; Moossa, A.R.; Katsuoka, K.; Hoffman, R.M. Hair Follicle–Derived Blood Vessels Vascularize Tumors in Skin and Are Inhibited by Doxorubicin. *Cancer Res.* **2005**, *65*, 2337–2343. [CrossRef]
55. Selleri, S.; Seltmann, H.; Gariboldi, S.; Shirai, Y.F.; Balsari, A.; Zouboulis, C.C.; Rumio, C. Doxorubicin-Induced Alopecia Is Associated with Sebaceous Gland Degeneration. *J. Investig. Dermatol.* **2006**, *126*, 711–720. [CrossRef]
56. Suchonwanit, P.; Thammarucha, S.; Leerunyakul, K. Minoxidil and its use in hair disorders: A review. *Drug Des. Devel. Ther.* **2019**, *13*, 2777–2786. [CrossRef]
57. Sharova, T.Y.; Poterlowicz, K.; Botchkareva, N.V.; Kondratiev, N.A.; Aziz, A.; Spiegel, J.H.; Botchkarev, V.A.; Sharov, A.A. Complex Changes in the Apoptotic and Cell Differentiation Programs during Initiation of the Hair Follicle Response to Chemotherapy. *J. Investig. Dermatol.* **2014**, *134*, 2873–2882. [CrossRef] [PubMed]
58. Wen, L.; Fan, Z.; Huang, W.; Miao, Y.; Zhang, J.; Liu, B.; Zhu, D.; Dai, D.; Zhang, J.; Le, D.; et al. Retinoic acid drives hair follicle stem cell activation via Wnt/β-catenin signalling in androgenetic alopecia. *Acad. Dermatol. Venereol.* **2025**, *39*, 189–201. [CrossRef] [PubMed]
59. Houschyar, K.S.; Borrelli, M.R.; Tapking, C.; Popp, D.; Puladi, B.; Ooms, M.; Chelliah, M.P.; Rein, S.; Pförringer, D.; Thor, D.; et al. Molecular Mechanisms of Hair Growth and Regeneration: Current Understanding and Novel Paradigms. *Dermatology* **2020**, *236*, 271–280. [CrossRef] [PubMed]
60. Nan, W.; Li, G.; Si, H.; Lou, Y.; Wang, D.; Guo, R.; Zhang, H. All-trans-retinoic acid inhibits mink hair follicle growth via inhibiting proliferation and inducing apoptosis of dermal papilla cells through TGF-β2/Smad2/3 pathway. *Acta Histochem.* **2020**, *122*, 151603. [CrossRef]
61. Osei-Sarfo, K.; Gudas, L.J. Retinoic Acid Suppresses the Canonical Wnt Signaling Pathway in Embryonic Stem Cells and Activates the Noncanonical Wnt Signaling Pathway. *Stem Cells* **2014**, *32*, 2061–2071. [CrossRef]
62. Benjamini, Y.; Hochberg, Y. Controlling the False Discovery Rate: A Practical and Powerful Approach to Multiple Testing. *J. R. Stat. Soc. Ser. B Stat. Methodol.* **1995**, *57*, 289–300. [CrossRef]
63. Schindelin, J.; Arganda-Carreras, I.; Frise, E.; Kaynig, V.; Longair, M.; Pietzsch, T.; Preibisch, S.; Rueden, C.; Saalfeld, S.; Schmid, B.; et al. Fiji: An open-source platform for biological-image analysis. *Nat. Methods* **2012**, *9*, 676–682. [CrossRef]
64. Niimori, D.; Kawano, R.; Felemban, A.; Niimori-Kita, K.; Tanaka, H.; Ihn, H.; Ohta, K. Tsukushi controls the hair cycle by regulating TGF-β1 signaling. *Dev. Biol.* **2012**, *372*, 81–87. [CrossRef]
65. Choi, Y.M.; Choi, S.Y.; Kim, H.; Kim, J.; Ki, M.S.; An, I.; Jung, J. TGFβ family mimetic peptide promotes proliferation of human hair follicle dermal papilla cells and hair growth in C57BL/6 mice. *Biomed. Dermatol.* **2018**, *2*, 23. [CrossRef]
66. Schmid, D.; Belser, E.; Zülli, F. The FGF7 and Noggin Genes are Key Targets to Treat Hair Loss. *SOFW-J.* **2013**, *139*, 9.
67. Kinoshita-Ise, M.; Tsukashima, A.; Kinoshita, T.; Yamazaki, Y.; Ohyama, M. Altered FGF expression profile in human scalp-derived fibroblasts upon WNT activation: Implication of their role to provide folliculogenetic microenvironment. *Inflamm Regen.* **2020**, *40*, 35. [CrossRef] [PubMed]
68. Imamura, T.; Oda, Y.; Oki, J.; Komi-Kuramochi, A.; Honda, E.; Asada, M.; Suzuki, M.; Kimura-Ueki, M. Telogen Phase of Hair Growth Cycle Is Regulated by Cyclic Epithelial FGF18 Signaling. *J. Dermatol. Sci.* **2013**, *69*, e64–e65. [CrossRef]
69. Wang, C.; Zang, K.; Tang, Z.; Yang, T.; Ye, X.; Dang, Y. Hordenine Activated Dermal Papilla Cells and Promoted Hair Regrowth by Activating Wnt Signaling Pathway. *Nutrients* **2023**, *15*, 694. [CrossRef] [PubMed]
70. Hendriks, M.; Ramasamy, S.K. Blood Vessels and Vascular Niches in Bone Development and Physiological Remodeling. *Front. Cell Dev. Biol.* **2020**, *8*, 602278. [CrossRef]
71. Mah, L.-J.; El-Osta, A.; Karagiannis, T.C. γH2AX as a molecular marker of aging and disease. *Epigenetics* **2010**, *5*, 129–136. [CrossRef]

72. Ivashkevich, A.; Redon, C.E.; Nakamura, A.J.; Martin, R.F.; Martin, O.A. Use of the γ-H2AX assay to monitor DNA damage and repair in translational cancer research. *Cancer Lett.* **2012**, *327*, 123–133. [CrossRef] [PubMed]
73. Garrison, C.M.; Schwarzbauer, J.E. Fibronectin fibril alignment is established upon initiation of extracellular matrix assembly. *MBoC* **2021**, *32*, 739–752. [CrossRef]
74. Speziale, P.; Arciola, C.R.; Pietrocola, G. Fibronectin and Its Role in Human Infective Diseases. *Cells* **2019**, *8*, 1516. [CrossRef]
75. Carraher, C.L.; Schwarzbauer, J.E. Regulation of Matrix Assembly through Rigidity-dependent Fibronectin Conformational Changes. *J. Biol. Chem.* **2013**, *288*, 14805–14814. [CrossRef]
76. Harshuk-Shabso, S.; Dressler, H.; Niehrs, C.; Aamar, E.; Enshell-Seijffers, D. Fgf and Wnt signaling interaction in the mesenchymal niche regulates the murine hair cycle clock. *Nat. Commun.* **2020**, *11*, 5114. [CrossRef]
77. Tripurani, S.K.; Wang, Y.; Fan, Y.-X.; Rahimi, M.; Wong, L.; Lee, M.-H.; Starost, M.F.; Rubin, J.S.; Johnson, G.R. Suppression of Wnt/β-catenin signaling by EGF receptor is required for hair follicle development. *MBoC* **2018**, *29*, 2784–2799. [CrossRef]
78. Wang, N.; Zhang, W.; Zhong, Z.; Zhou, X.; Shi, X.; Wang, X. FGF7 secreted from dermal papillae cell regulates the proliferation and differentiation of hair follicle stem cell1. *J. Integr. Agric.* **2023**, S2095311923003544. [CrossRef]
79. Suthon, S.; Perkins, R.S.; Bryja, V.; Miranda-Carboni, G.A.; Krum, S.A. WNT5B in Physiology and Disease. *Front. Cell Dev. Biol.* **2021**, *9*, 667581. [CrossRef]
80. Reddy, S.; Andl, T.; Bagasra, A.; Lu, M.M.; Epstein, D.J.; Morrisey, E.E.; Millar, S.E. Characterization of Wnt gene expression in developing and postnatal hair follicles and identification of Wnt5a as a target of Sonic hedgehog in hair follicle morphogenesis. *Mech. Dev.* **2001**, *107*, 69–82. [CrossRef] [PubMed]
81. Xu, X.; Lyle, S.; Liu, Y.; Solky, B.; Cotsarelis, G. Differential Expression of Cyclin D1 in the Human Hair Follicle. *Am. J. Pathol.* **2003**, *163*, 969–978. [CrossRef] [PubMed]
82. van der Maaten, L.; Postma, E.; Herik, H. Dimensionality Reduction: A Comparative Review. *JMLR* **2007**, *10*.
83. Ashburner, M.; Ball, C.A.; Blake, J.A.; Botstein, D.; Butler, H.; Cherry, J.M.; Davis, A.P.; Dolinski, K.; Dwight, S.S.; Eppig, J.T.; et al. Gene Ontology: Tool for the unification of biology. *Nat. Genet.* **2000**, *25*, 25–29. [CrossRef]
84. Liu, H.; Chen, B.; Lilly, B. Fibroblasts potentiate blood vessel formation partially through secreted factor TIMP-1. *Angiogenesis* **2008**, *11*, 223–234. [CrossRef]
85. Jia, G.; Aroor, A.R.; Jia, C.; Sowers, J.R. Endothelial cell senescence in aging-related vascular dysfunction. *Biochim. et Biophys. Acta (BBA)-Mol. Basis Dis.* **2019**, *1865*, 1802–1809. [CrossRef]
86. Simms, V.A.; Bicknell, R.; Heath, V.L. Development of an ImageJ-based method for analysing the developing zebrafish vasculature. *Vasc. Cell* **2017**, *9*. [CrossRef]
87. Perié, L.; Houël, C.; Zambon, A.; Guere, C.; Vié, K.; Leroy-Dudal, J.; Vendrely, C.; Agniel, R.; Carreiras, F.; Picot, C.R. Impaired incorporation of fibronectin into the extracellular matrix during aging exacerbates the senescent state of dermal cells. *Exp. Cell Res.* **2024**, *442*, 114251. [CrossRef] [PubMed]
88. Siddiqui, M.S.; François, M.; Fenech, M.F.; Leifert, W.R. Persistent γH2AX: A promising molecular marker of DNA damage and aging. *Mutat. Res./Rev. Mutat. Res.* **2015**, *766*, 1–19. [CrossRef]
89. Headington, J.T. Hair Follicle Biology and Topical Minoxidil: Possible Mechanisms of Action. *Dermatology* **1987**, *175*, 19–22. [CrossRef] [PubMed]
90. Lachgar; Charveron; Gall; Bonafe Minoxidil upregulates the expression of vascular endothelial growth factor in human hair dermal papilla cells. *Br. J. Dermatol.* **1998**, *138*, 407–411. [CrossRef] [PubMed]
91. Michelet, J.-F.; Commo, S.; Billoni, N.; Mahé, Y.F.; Bernard, B.A. Activation of Cytoprotective Prostaglandin Synthase-1 by Minoxidil as a Possible Explanation for Its Hair Growth-Stimulating Effect. *J. Investig. Dermatol.* **1997**, *108*, 205–209. [CrossRef]
92. Wang, A.S.; Dreesen, O. Biomarkers of Cellular Senescence and Skin Aging. *Front. Genet.* **2018**, *9*, 247. [CrossRef]
93. Rossetti, D.; Kielmanowicz, M.G.; Vigodman, S.; Hu, Y.P.; Chen, N.; Nkengne, A.; Oddos, T.; Fischer, D.; Seiberg, M.; Lin, C.B. A novel anti-ageing mechanism for retinol: Induction of dermal elastin synthesis and elastin fibre formation: Retinol induces elastin synthesis. *Int. J. Cosmet. Sci.* **2011**, *33*, 62–69. [CrossRef] [PubMed]
94. Raja, E.; Clarin, M.T.R.D.C.; Yanagisawa, H. Matricellular Proteins in the Homeostasis, Regeneration, and Aging of Skin. *IJMS* **2023**, *24*, 14274. [CrossRef] [PubMed]

Disclaimer/Publisher's Note: The statements, opinions and data contained in all publications are solely those of the individual author(s) and contributor(s) and not of MDPI and/or the editor(s). MDPI and/or the editor(s) disclaim responsibility for any injury to people or property resulting from any ideas, methods, instructions or products referred to in the content.